JOURNAL OF MATERIALS SCIENCE 13 (1978) 1749–1760

Cracking and toughening of concrete and polymer-concrete dispersed with short steel wires

PETER W. R. BEAUMONT, JAMES C. ALESZKA*
Department of Engineering, University of Cambridge, Cambridge, UK

A fibre-strengthened brittle solid can crack and fracture in a number of ways and simple models can be used to describe quantitatively the fracture processes. This paper discusses some of these models and compares experimental measurements of cracking stress and toughness for two brittle fibrous composites with the theoretical predictions. The two brittle matrices are concrete and concrete impregnated with polymethylmethacrylate reinforced by discontinuous (short) high strength steel wires. It involved extracting a single steel wire from each brittle matrix to evaluate the debonding stress and pull-out stress as a function of fibre embedded length. These key material parameters and the energetics of cracking determined in three-point flexural experiments, together with the cracking and toughening equations are then used to characterize the fracture behaviour of fibre-strengthened concrete and polymer–concrete composites.

1. Introduction

It may be convenient to think of a solid as having a unique fracture stress, below which it does not crack, but this is generally not true. In polycrystalline solids, the mechanisms of crack growth lead to all the common modes of failure, cleavage, ductile, trans- and intergranular fracture, etc., and in glassy polymers the cavitation process of fracture is generally recognized as the initial stage of practically all the micromechanical regimes of cracking. But when a strong fibre is dispersed throughout a ductile or brittle matrix, a multiplicity of quite different microfracture processes can occur. In a fibre-strengthened brittle solid (carbon fibres in glass or steel wires in concrete, for instance), at least five distinguishable mechanisms are possible [1–9], each process contributing to the toughness of the fibrous composite. These microscopical crack growth mechanisms can combine in various ways to give different combinations of macroscopic fracture behaviour.

This paper presents some experimental measurements of cracking stress and toughness for two brittle materials containing a dispersion of short, high strength steel wires. The matrices are concrete and concrete that has been impregnated with polymethylmethacrylate (PMMA). The object is to evaluate the effects of the PMMA on the fibre debond stress and fibre pull-out stress, and the influence on the cracking stress and fracture toughness of the steel wire-reinforced concrete composite. We offer some discussion of the revelant cracking mechanisms described in [1–9], and their limitations in quantitatively describing the observed cracking stresses and toughness of these composite materials.

Our approach has been to use the existing models and to experimentally determine those terms in the analyses that are relatively easy to obtain; and to make simple assumptions of other parameters which we have been unable to evaluate. This involved carrying out single steel wire pull-out experiments to determine debonding and pull-out stresses, and then carrying out three-point flexural tests on prismatic bars to evaluate the first cracking stress and post-cracking stength of the fibrous composite and its fracture toughness.

*Effects Technology Inc., 5383 Hollister Avenue, P.O. Box 30400, Santa Barbara, California 93105, USA.

2. Cracking stress and toughness equations

In this section, we list the relevant equations used to calculate the cracking stresses and toughness of a brittle solid containing a dispersion of short ductile fibres, together with a brief explanation. The equations selected are based on physically sound microscopic fracture models. Frequently, this leads to an equation containing one or more terms for which only bounds are known or can be found. Theory provides the form of the equation and we then have to resort to experimental data in order to determine the constants which enter it.

2.1. Matrix cracking

In this case, the presence of ductile fibres in a brittle matrix can increase the stress to nucleate the first matrix crack. The onset of cracking results in a localized release of elastic strain energy in the matrix; it may also (and frequently does) involve the breakdown of the fibre–matrix interface (debonding) on either side of the matrix crack which, if it occurs, results in the dissipation of energy in fibre–matrix sliding and an increase in local elastic strain energy in the adjacent fibres; new fracture surfaces form in the matrix; and finally, the applied stress does additional work on the matrix due to an increase in compliance of the cracked composite [1]. Matrix relaxation occurs over a distance which depends upon fibre diameter (d) and fibre volume fraction (V_f); and the critical strain in the matrix at the first cracking stress of an aligned fibrous composite is given by

$$\epsilon_m = [24\gamma_m \tau E_f V_f^2 / E_m^2 E_c d(1 - V_f)]^{1/3} \quad (1)$$

γ is fracture surface energy and E is Young's modulus; the subscripts m, f and c refer to the matrix, fibre and composite, respectively. τ is the interfacial shear strength. This model is for the non-elastic case where there is no connection between the elastic displacements in the fibre and in the matrix, and it assumes interfacial breakdown on either side of the matrix crack, without fibre breakage.

The second criterion for the matrix to crack is that the stress on the composite at the first crack is less than the load carried by the fibres per unit area of composite, i.e.

$$\epsilon_m E_c \leqslant \sigma_f V_f \quad (2)$$

where σ is the tensile stress and $E_c = E_f V_f + E_m(1 - V_f)$. We see that the first cracking stress is inversely proportional to $d^{1/3}$ and depends upon τ, E_f and γ_m. The first cracking stress can be reached provided

$$l/d \geqslant E_c \epsilon_m / \tau V_f \quad (3)$$

where l is the length of the fibre.

In the elastic case, where fibre and matrix remain intact without interfacial sliding (which is unlikely in the case of steel wire/concrete composites) then [10]

$$\epsilon_m^2 = [(4\gamma_m(1 - V_f)/dE_c\alpha) \times 2G_m E_c / \psi E_f E_m (1 - V_f)]^{1/2} \quad (4)$$

where G is the shear modulus, $\alpha = E_m(1 - V_f)/E_f V_f$, and the spacing between fibres $\psi = \ln(\pi/2\sqrt{3}V_f)^{1/2}$. The first cracking stress can then be written as

$$\sigma_m = [4E_m\gamma_m/d(1 + \alpha)]^{1/2} \times [2G_m E_c / \psi E_f E_m (1 - V_f)]^{1/4} \quad (5)$$

The cracking stress is proportional to the product $(E_m\gamma_m)^{1/2}$; and it is inversely proportional to fibre spacing and depends also on fibre volume fraction.

2.2. Fracture stress limited by interface friction

When the brittle matrix first cracks, the fibre–matrix interface can be expected to debond. The ultimate fracture stress of the composite will then depend upon the forces to overcome the friction between fibre and matrix during fibre pull-out. It presupposes that the strength of the fibres $\sigma_f > \sigma_c/V_f$ and that the post-cracking stress exceeds the first cracking stress.

The frictional resistance to the fibre pulling out depends upon the normal compressive forces exerted by the matrix on the fibre; it will also depend upon the radial deformation of the fibre by the matrix. A tensile load on the fibre will cause it to contract laterally and reduce the frictional force accordingly [11–14]. A semi-empirical expression for the tensile stress on a fibre during pull-out is [15]

$$\sigma_f = (\tau_0/k)[1 - \exp(-4kl_e/d)] \quad (6)$$

where τ_0 is the limiting interfacial bond strength ignoring Poisson contraction of the fibre; k is a fitting constant and l_e is the embedded length of fibre. Extending the argument that the shear stress at the interface decreases linearly with stress on the fibre, then the composite post-cracking

strength is

$$\sigma_c = (V_f \tau_0 / k) \times [1 + (d/2lk) \exp(-2lk/d) - (d/2lk)] . \quad (7)$$

The parameter k can be equated to the physical material parameters that take into account the effect of Poisson contraction of the fibre during pull-out and the effect of compression of the matrix upon the fibre [11, 13];

$$k = E_m \nu_f \mu / E_f (1 + \nu_m) \text{ (Takaku and Arridge)} \quad (8)$$

and

$$k = \nu_f \mu / E_f \times [(1 + \nu_m / E_m) + (1 - \nu_f / E_f)] \text{ (Pinchin)} \quad (9)$$

ν is Poisson's ratio and μ is the coefficient of friction between fibre and matrix.

Any fibres which are misoriented with respect to the direction of applied stress will straighten out by a plastic shearing process provided $l/d = \epsilon_m E_c / \tau V_f$. If the fibre pull-out force is relatively insensitive to the angle through which such a fibre is plastically deformed [16, 17] then the tensile strength of a brittle matrix containing randomly oriented fibres in two-dimensions only will be given by Equation 7 multiplied by a factor of less than one to take into account the actual number of fibres crossing the matrix fracture plane [10].

2.3. Fibre pull-out energy

At the maximum post-cracking load, those fibre ends that lie less than $l/2$ from the matrix crack plane will begin to pull out under decreasing load, provided the embedded length is less than $d\sigma_f/4\tau$. For a fibrous composite containing fibres of length $l < d\sigma_f/2\tau$, then all of the fibres will pull out rather than fracturing; provided $l > d\sigma_f/2\tau$, then only a fraction (l_c/l) will pull out, and the remainder will break when the stress on the fibre exceeds the fibre strength. (l_c is a critical fibre length and is defined as the minimum length of fibre that can be loaded to its breaking load).

The toughness of discontinuous fibrous composites may be equated to the work done in pulling the fibres out of their matrix sockets against a frictional shear stress τ' at the interface [2–4],

$$\gamma_p = V_f \tau' l^2 / 12d \quad (l < d\sigma_f/2\tau) \quad (10)$$

and

$$\gamma_p = V_f \sigma_f^3 d / 12\tau'^2 \quad (l > d\sigma_f/2\tau) \quad (11)$$

2.4. Plastic shearing of ductile fibres

In this case, those fibres "bridging" a matrix crack which are misoriented with respect to the tensile stress direction, will straighten out by a plastic shearing process provided $l/d = \epsilon_m E_c / \tau V_f$. The work done in plastically deforming the fibre is [18]

$$W = f(V_f, l, \theta) \int_0^{\epsilon_f} \sigma \, d\epsilon \quad (12)$$

where l is the length of the plastically deformed volume of fibre. A metal fibre lying at an angle θ to the matrix crack plane will be pulled out of a matrix crack face; simultaneously, it will be plastically sheared along its entire pulled out length. The effect of plastic flow on the toughness of the composite can be shown to be [5, 6]

$$\gamma_s = V_f \tau_y \theta l / 8 \quad \text{approximately} \quad (13)$$

where τ_y is the yield stress of the ductile fibre. (It is assumed that all of the fibres pull-out leaving fibre ends protruding above the fracture surface of the matrix between 0 and $l/2$ in length).

3. Experimental procedure and analysis

3.1. Materials

Brass-coated steel wire was used as the reinforcement in concrete or concrete impregnated with polymethylmethacrylate (PMMA); the wire has a tensile yield stress of about 590 MN m^{-2} and an average ultimate tensile stress of about 2.1 GN m^{-2}. The proportion of cement, sand, and water used in the processing of the concrete was 3 : 7 : 1 parts by weight. A known amount of short steel wires of a particular length and diameter were mixed in with the mortar; the length of wire was either 12.5 mm, 19 mm, 25 mm or 37 mm with a diameter of either 0.25 mm, 0.40 mm or 0.5 mm, giving ratios of l/d between 25 and 148. The resulting concrete mix, containing up to 3% by volume approximately of steel wire, was then cast into individual moulds 12.5 cm long, with a square cross-section of 2.5 cm x 2.5 cm. All of the "as-cast" samples were placed into polyethylene bags containing water, and the bags were then sealed. Curing of the concrete samples took place over the next 28 days at room temperature. At the end of this period, the samples were dried overnight at a temperature between 105 and 150° C. About one-half of the

cured concrete samples were placed inside a chamber; liquid methylmethacrylate monomer was then added and the chamber pressurized at about 280 kN m^{-2}. After about 2 hours, the pressure was released and the excess monomer drained off. All of the samples were then wrapped in aluminium foil and heated to 70° C. For the steel wire/PMMA-impregnated concrete composite, the amount of PMMA in the concrete was 15% by volume approximately; to other samples of concrete without the steel wires, were added different amounts of PMMA, during the mixing stage, up to 18% by volume. Some of the specimens were exposed to sea water for up to 6 months before testing; others were exposed to sea water for 6 weeks and then at −20° C for 48 h.

3.2. Specimen design and analysis

Prismatic bars 12.5 cm long with a square cross-section 2.5 cm × 2.5 cm were cast out of concrete and PMMA-impregnated concrete, with and without dispersions of short steel wires. Some of the bars were notched at the midpoint to a depth of 5 mm using a 0.5 mm thick diamond cutting wheel. Each specimen was then loaded in turn in three-point flexure at a displacement rate of 1.25 mm min^{-1}. The specimen span : depth ratio was kept constant at 4 : 1. Some specimens were pre-cracked and then exposed to sea water for 6 months before carrying out the flexural test. A minimum of 5 duplicate tests were completed for each group of specimens.

3.2.1. Modulus of rupture

The un-notched beams were used to evaluate the first cracking stress and modulus of rupture (MOR) (or post-cracking stress) where

$$\text{MOR} = 3P_{\max}L/2bd^2 \qquad (14)$$

$P_{\max}$ is the highest load recorded in the flexural test, L is the span (= 10 cm) and b and d are the breadth and depth of the beam, respectively.

Since failure occurred by the initiation and propagation of a single crack followed by fibre pull-out, then the bending moment M is given by $\sigma bd^2/2$ where σ is equal to the load on the fibres bridging the matrix crack divided by the unit area of crack face. For elastic behaviour, the modulus of rupture is given by Equation 14 and it follows that MOR = 3σ. A value of 2.7 has been calculated by Aveston *et al.* [15] for steel wire-reinforced concrete and is the value that we have used when comparing MOR values with the theory of tensile strength.

3.2.2. Plane strain fracture toughness (K_{IC})

In this test, the single edge notched specimen was loaded in flexure and the plane strain fracture toughness (K_{IC}) of concrete and PMMA-impregnated concrete determined using the equation

$$K_{IC} = Y3P_{\max}La^{1/2}/2bd^2 \qquad (15)$$

where a is the notch depth and Y is a polynomial in notch ratio which takes into account the effects of finite sample size on the crack tip stress field:

$$Y = 1.93(a/d)^{1/2} - 3.07(a/d)^{3/2} + 14.53(a/d)^{5/2} - 25.11(a/d)^{7/2}$$

3.2.3. Fracture surface energy (γ_m)

The fracture surface energy of the matrix was calculated using the relationship

$$\gamma_m = K_{IC}^2/2E_m \quad \text{approximately} \qquad (16)$$

and experimental values of K_{IC} and E_m measured in flexure.

3.2.4. Work of fracture (γ_F)

Work of fracture measurements were made by integrating the load/deflection curve and equating this to the total work (U) to propagate a single crack through the composite; the work of fracture is simply defined as

$$\gamma_F = (U/2A) \qquad (17)$$

where $2A$ is the total apparent area of the two newly created fracture surfaces.

3.2.5. Interfacial shear strength

Single fibre pull-out tests were carried out using a 0.5 mm diameter steel wire embedded in a block of the matrix 5 cm by 1 cm by 1 cm. The embedded fibre length (l_e) was varied between 6 mm and 50 mm and the fibre was pulled out using a displacement rate of 1.25 mm min^{-1}.

In this test, a maximum interfacial shear stress is reached at the point where the fibre enters the matrix ($x = l_e$). Provided the shear strength of the interface is exceeded, then debonding will result, and the debonded zone will spread along the embedded length of fibre. The debonding stress and pull-out stress can be estimated using a shear lag analysis [11, 19] and the experimental data

obtained from the fibre pull-out experiments. The relationship between the tensile stress on the fibre for debonding (σ_d) and embedded fibre length is given by

$$\sigma_d = (4\tau_{max}/d\alpha)(\tanh \alpha l_e) \quad (18)$$

where the material constant $\alpha = (4H/dE_f)^{1/2}$ and $H = 2\pi G_m/\ln(r_m/r_f)$; r_m is the radius of a concentric cylinder of matrix around the fibre of radius r_f.

The average shear stress (τ_{av}) is given by

$$\tau_{av} = d\sigma_d/4l_e. \quad (19)$$

Since the interfacial shear stress reaches a maximum value at the point where $x = l_e$ then the ratio τ_{av}/τ_{max} is simply

$$\tau_{av}/\tau_{max} = (\alpha l_e)^{-1}(\tanh \alpha l_e) \quad (20)$$

As the embedded length of wire tends towards zero ($l_e \to 0$), then τ_{av}/τ_{max} tends towards unity, i.e. τ_{av} tends towards τ_{max}.

The maximum or limiting value of the interfacial shear stress can be estimated by plotting the experimental values of τ_{av} against l_e, and extrapolating a curve through these points to cut the τ_{av} axis at $l_e = 0$. For any embedded length of fibre, τ_{av}/τ_{max} can be determined; a corresponding value of αl_e can be obtained using Equation 20.

4. Results and discussion

4.1 Single fibre pull-out experiments

4.1.1. Debonding limited by interfacial friction

The general shape of the load/extension curve obtained by extracting a single steel wire out of a block of concrete or polymer–concrete is shown in Fig. 1. Two important stresses are defined; the first corresponds to the tensile stress on the wire at the onset of debonding, σ_d, and is simply the maximum load divided by the cross-sectional area of the wire; the second stress, σ_p, is the initial tensile stress on the wire as the wire begins to pull out of the matrix. Both stresses were determined experimentally for various embedded lengths of steel wire and these are shown in Figs. 2 and 3. Impregnation of the concrete with PMMA has significantly increased the values of σ_d and σ_p.

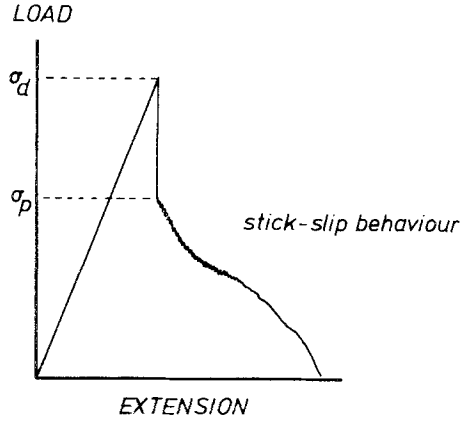

Figure 1 A typical load/extension curve obtained during the extraction of a single steel wire from concrete or PMMA concrete.

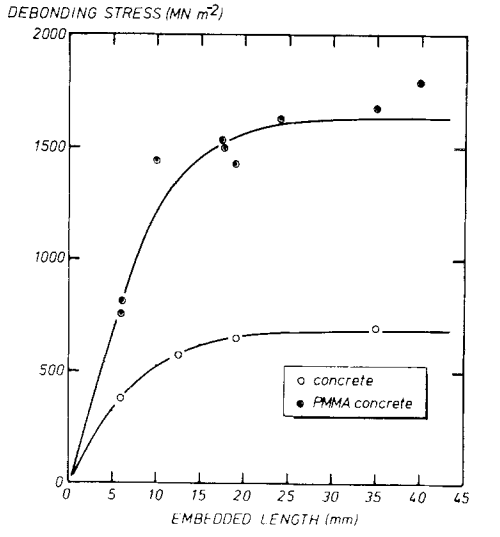

Figure 2 Experimental values of debonding stress as a function of embedded fibre length for concrete and PMMA concrete. The solid curves were calculated using Equation 18.

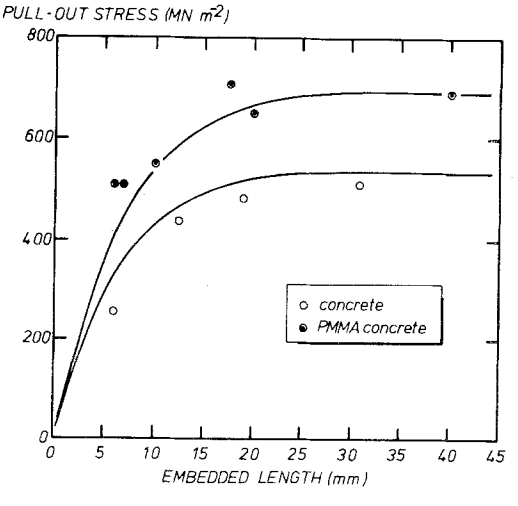

Figure 3 Experimental values of pull-out stress as a function of embedded fibre length for concrete and PMMA concrete. The solid curves were calculated using Equation 21.

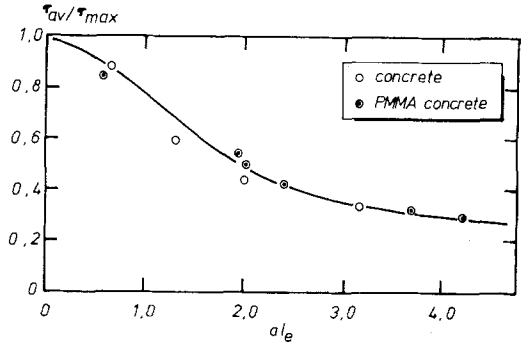

Figure 4 Comparison of experimental results of τ_{av}/τ_{max} as a function of αl_e for concrete and PMMA concrete with theoretical prediction using Equation 20.

The non-linear relationship between debonding stress and embedded length and pull-out stress and embedded length can be related to the elastic shear stress distribution.

The relationship betweeen fibre debonding stress and embedded length was determined by inserting the appropriate value of α and τ_{max} into Equation 18. First, the maximum or limiting value of the interfacial shear stress was estimated by extrapolating a curve through the experimental data of τ_{av}, plotted against l_e so as to intersect the τ_{av} axis at $l_e = 0$. Next a value for α was selected so that a plot of Equation 20 fitted the experimental data and this is shown in Fig. 4, where τ_{av}/τ_{max} is plotted as a function of αl_e. The average interfacial shear stress was calculated using Equation19 and the experimental values of σ_d. The values for α and τ_{max} obtained in this way are shown in Table I. Impregnation of concrete with PMMA has raised the limiting value of the interfacial shear strength from 9 MN m^{-2} to 19.5 MN m^{-2}, approximately.

TABLE I

Parameter	Concrete	PMMA Concrete
α (m^{-1})	95	105
τ_{max} (MN m^{-2})	9.0	19.5

4.1.2. Pull-out limited by interfacial friction

The resistance to the extraction of the wire is due to shrinkage of the matrix during curing. Under a tensile force, the wire will contract laterally, the compressive force exerted by the matrix will be reduced, and the frictional force at the interface will then decrease. If we also consider the radial deformation of the wire brought about by the contracting concrete, then the dependence of the initial pull-out stress on the wire of embedded length, l_e, is of the form

$$\sigma_p = A\,[1 - \exp(-Bl_e)] \qquad (21)$$

where

$$A = \sigma_0/k = E_f\epsilon_0/k$$

$$B = 4k\mu/d \quad \text{and}$$

$$k = v_f\mu/E_f\,[(1 + v_m/E_m) + (1 - v_f/E_f)]$$

σ_0 is the compressive stress on the wire due to shrinkage in the matrix, and ϵ_0 is the original strain in the matrix. μ is the coefficient of friction between the steel wire and matrix. This expression is similar in form to the semi-empirical relationship derived by Aveston *et al.* [15] (Equation 6). We have determined the values of A and B by a graphical method and present them in Table II.

A plot of Equation 21 is found to fit the experimental data extremely well (Fig. 3). This gives a value for $\mu = 0.6$ for the two concretes which is

TABLE II

Parameter	Concrete	PMMA concrete
A (MN m^{-2})	537	676
B (m^{-1})	171	231
k	0.036	0.048
σ_0 (MN m^{-2})	19.2	32.6
μ	0.6	0.6

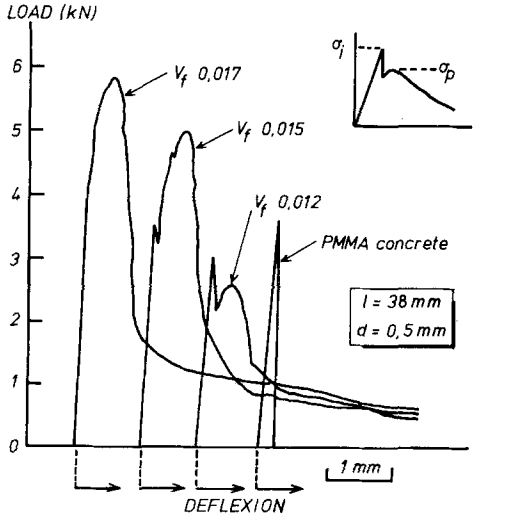

Figure 5 Some typical load/deflection curves obtained during three-point bending tests on concrete or PMMA concrete. The examples given are for PMMA concrete. (The insert defines the first cracking stress, σ_i, and post-cracking stress, σ_p).

reasonable. The parameters A and B are slightly different for the two samples which reflects the differences in properties of the two matrices.

4.2. Cracking stresses in flexure

4.2.1. First cracking stress limited by interfacial friction

The general shapes of load/deflection curves obtained in flexural tests on concrete and PMMA-impregnated concrete dispersed with short steel wires are typified in Fig. 5; the insert in the figure defines the first cracking stress and maximum post-cracking stress. The first signs of cracking are heard when the fracture strain of the matrix is exceeded; the value depends upon the parameters that appear in Equation 1. Some typical measurements of the first cracking stress for PMMA-impregnated concrete dispersed with steel wires are shown in Fig. 6. Data plotted in this way show a wide spread of observed first cracking stresses. By combining Equations 1 and 2 we get for the first cracking stress

$$\sigma_c = [24\gamma_m \tau E_f V_f^2 / E_m^2 E_c d(1 - V_f)]^{1/3} E_c \quad (22)$$

for non-elastic behaviour and see that the first cracking stress is inversely proportional to $d^{1/3}$ and depends slowly on fibre volume fraction. This equation suggests incorrectly that the first cracking stress of the composite decreases to zero as $V_f \to 0$. The results indicate that the first cracking stress tends to the first cracking stress of the unreinforced matrix at small values of V_f (i.e. at $V_f < V_{fcrit}$). If the data are normalized with respect to fibre diameter and replotted against V_f (Fig. 7) the spread is reduced significantly, and the predicted first cracking stress agrees remarkably well with the measured values (provided $V_f > V_{fcrit}$). Similarly, a plot of first cracking stress against wire diameter (d) shows a close agreement between the predicted values and experimental observation (Fig. 8). For completeness' sake, we have presented both the non-elastic and fully elastic models (Equations 22 and 5) and it is seen that the two models agree well at small values of d

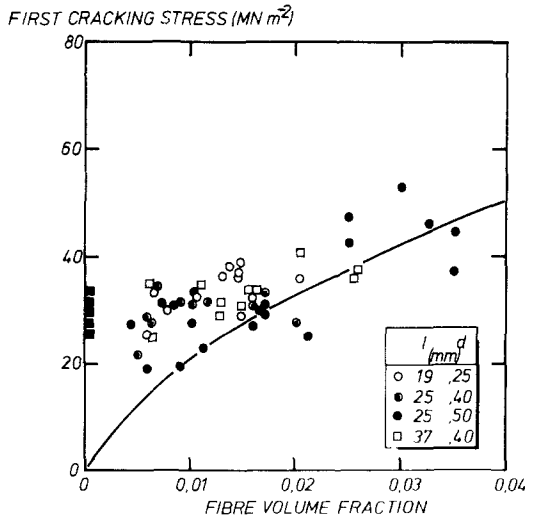

Figure. 6 Some typical first cracking stress data for PMMA concrete as a function of fibre volume fraction. The solid curve was calculated using Equation 22. The ■ points indicate the cracking stress of PMMA concrete.

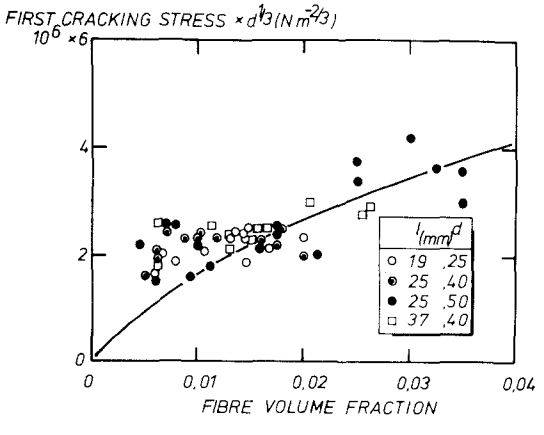

Figure 7 Some normalized first cracking stress data with respect to $d^{1/3}$ for PMMA concrete plotted against fibre volume fraction. The solid curve was calculated using Equation 22.

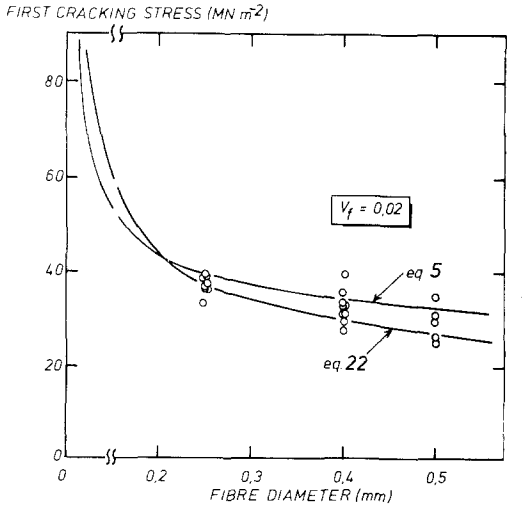

Figure 8 Some first cracking stress data for PMMA concrete as a function of fibre diameter ($V_f = 0.02$). The solid curves were calculated using Equations 5 and 22.

TABLE III

Parameter	Concrete	PMMA concrete
Young's modulus (E_m) (GN m^{-2})	34.0	44.1
Poisson's ratio (ν)	0.27	0.22
Shear modulus (G_m) (GN m^{-2})	13.4	19.7
Fracture surface (γ_m) (J m^{-2})	1.75	20.0
Interfacial shear strength (τ) (MN m^{-2})	9.0	19.5

but begin to deviate slightly from one another at higher values of d. Values for the constants which appear in these two equations are listed in Table III.

4.2.2. Post-cracking stress limited by interfacial friction

The post-cracking strength of an aligned discontinuous fibrous composite can be calculated from the fibre pull-out force to extract embedded fibres of lengths between 0 and $l/2$ from the plane of the matrix crack (Equation 7);

$$\sigma_c = (V_f\tau_0/k)(1 + d/2lk \exp(-2lk/d) - d/2lk)$$

k is given by Equation 8 or 9.

All of the experimental values of maximum post-cracking stress have been plotted in a normalized form as a function of the fibre aspect ratio (l/d) (Fig. 9). The values of τ_0 and k used in Equation 7 are listed in Table IV. The choice of these particular values allows Equation 7 to

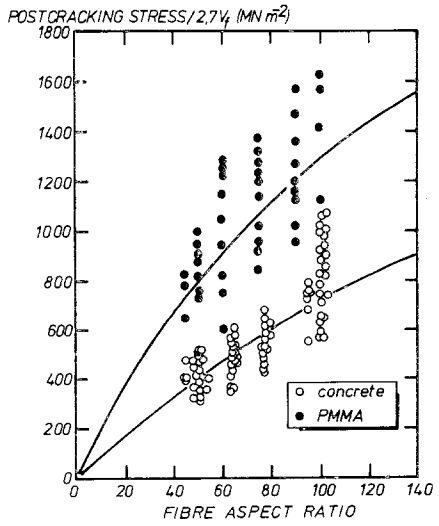

Figure 9 All of the post-cracking stress data normalized with respect to V_f as a function of fibre aspect ratio (l/d). The solid curves were calculated using Equation 7. (The constant 2.7 is the ratio MOR/σ_c).

TABLE IV

Parameter	Concrete	PMMA concrete
τ_0 (MN m^{-2})	9	19.5
k	0.004	0.007
μ	0.12	0.17

predict the observed post-cracking stresses reasonably accurately. The limiting value of interfacial shear stress is identical to the value of the maximum interfacial shear stress, τ_{max}, obtained in the single fibre pull-out experiments (Table I). Assuming that E_f, E_m, ν_m and ν_f are well characterized parameters (Table III), then the values of k chosen for the concrete composite and PMMA-impregnated composite suggest coefficients of friction, μ, equal to about 0.12 and 0.17 respectively, which are about 4 times less than the values obtained in the single fibre pull-out experiments. Similar observations were made by Pinchin [13].

Examination of the fracture surfaces showed the majority of holes from which steel wires had been extracted to be of circular cross-section rather than being elliptical in shape. This indicates that most of the fibres were aligned or were only slightly misoriented with respect to the principal stress direction. The effective fibre volume fractions were evaluated by inspection of every fracture face of specimens broken. It was found that over 90% of the total fibre content intersected the plane of the crack. This is a much higher proportion than the $2/\pi$ fraction estimated by Aveston and Kelly [10] for a perfectly random two-dimensional array of fibres. For this reason, the factor of $2/\pi$ to take into account a two-dimensional array of steel wires can be neglected in the analysis of post-cracking stress. The factor of 2.7 appears in the analysis so that the results of the flexural tests can be compared directly with the model.

Exposure of pre-cracked samples to sea water for 6 weeks followed by freezing at -20° C for 48 h had no effect whatsoever on the post-cracking strength of the polymer-impregnated composite.

4.2.3. Critical fibre volume fraction (V_f^*)

A critical fibre volume fraction, V_f^*, can be defined where the first cracking stress is equal to the post-cracking stress; it defines a minimum volume fraction of fibres below which fibre-strengthening beyond the first cracking stress does not occur. If we equate, therefore, the two equations defining these two cracking stresses (Equations 7 and 22)

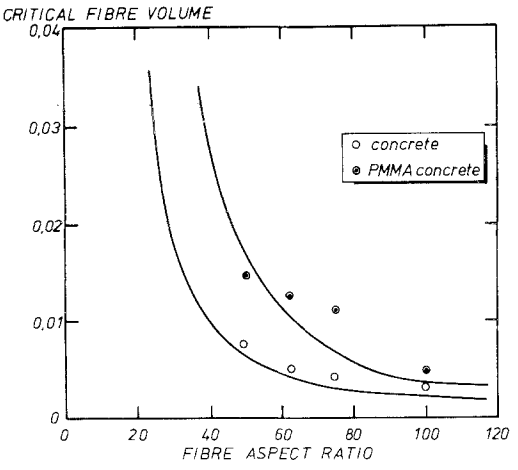

Figure 10 Some critical fibre volume fraction (V_f^*) data as a function of fibre aspect ratio (l/d). The solid curves were calculated using Equation 23.

and solve for V_f^*, we get

$$V_f^* = 24\gamma_m E_f k^3/d\tau^2 \,[1 + d/2kl \exp(-2kl/d) - d/2kl] \text{ approximately} \quad (23)$$

(We are taking $E_c \approx E_m$ and $V_m \approx 1$ when $V_f < 0.05$). Inserting the appropriate values into Equation 23 and plotting V_f^* against l/d shows good agreement with experimental observations (Fig. 10). It can be seen that V_f^* becomes increasingly more sensitive to l/d as the ratio falls below about 80. A greater amount of fibre is necessary in the PMMA-impregnated concrete matrix than in the plain concrete for the post-cracking strengthening effect to be observed.

4.3. Energies of crack propagation

4.3.1. Concrete and PMMA-impregnated concrete

The fracture surface energy, γ_m, and plane strain fracture toughness, K_{IC}, of concrete as a function of the volume fraction of PMMA is shown in Fig. 11. An addition of about 18% by volume of PMMA increases γ_m by more than 20 times. The relationship between γ_m and V_f (PMMA) does not appear to be linear, and the fracture surface energy of the polymer–concrete is less than would have been predicted assuming a rule-of-mixtures relationship between fracture energy and volume fraction of the two phases. A change in mode of crack propagation in concrete was observed after adding about 18% (by volume) PMMA; in the plain concrete intergranular fracture occurred by the propagation

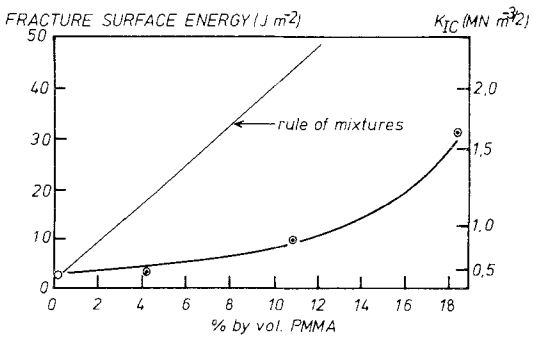

Figure 11 Fracture surface energy (γ_m) and plane strain fracture toughness (K_{IC}) data for concrete plotted against % vol. PMMA. The solid curve was calculated assuming a rule of mixtures to predict the fracture surface energy of the two-phase system.

Figure 12 Fracture surface of plain concrete.

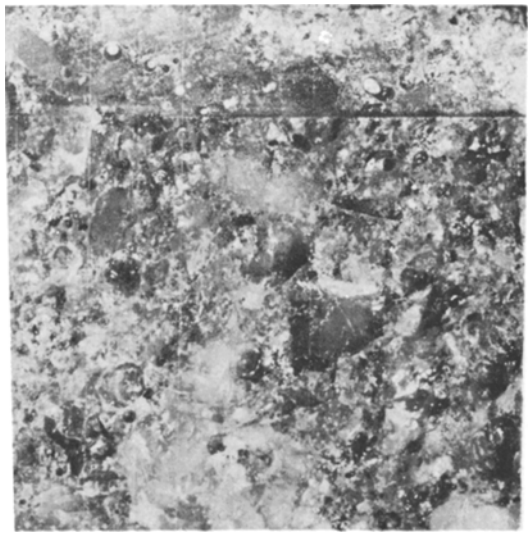

Figure 13 Fracture surface of concrete containing 18% (by vol.) PMMA.

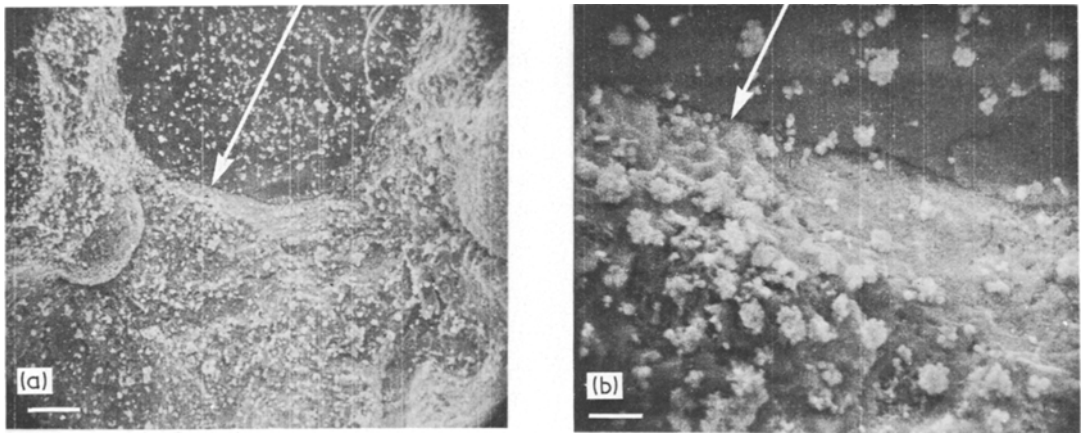

Figure 14 Interface cracking in PMMA concrete after exposure to sea water for 6 months. (a) The marker line represents 50 μm; (b) The marker line represents 10 μm.

of a crack around the aggregate particles, whereas in the PMMA-filled solid, transgranular fracture predominated by the breakage of these aggregate dispersions. It suggests that the presence of PMMA increases the bond strength between aggregate and matrix, and inhibits interfacial breakdown as well as filling pores. Typical fracture surface appearances are shown in Figs. 12 and 13.

4.3.2. Environmental effects

Exposure to sea water for up to 6 months resulted in the concrete and PMMA-concrete matrices picking up about 2.4% (by wt) and 1.6% (by wt) of water, respectively [20]. A comparison between these values and the amount of water picked up by the fibrous composite (2.3% by vol.) shows that the polymer–concrete is more resistant to the absorption of water than the other two materials. The gain in weight may be directly related to the porosity; the more porous the matrix, the greater will be the amount of water picked up. Since the polymer filled the majority of the voids in the concrete (cf. Figs. 12 and 13) then the lower weight gain for the PMMA-concrete should not be unexpected. Microscopic examination of the fracture surface of the PMMA-concrete matrix after 6 months exposure to sea water showed a rougher topography and some aggregate–matrix separation (debonding) (Fig. 14). A corresponding decrease in fracture toughness by a factor of three was observed [20].

4.3.3. Work of fracture; the dependence on interfacial friction

Since the majority of fibres were aligned, theoretical estimations of the work of fracture can be made using the fibre pull-out model (Equation 10);

$$\gamma_p = V_f \tau' l^2 / 12d$$

Figs. 15 and 16 show normalized plots of Equation 10 against fibre volume fraction together with all of the work of fracture data collected. Thus a plot of $12d\gamma_p/l^2$ against V_f should produce a straight line, the slope of which is equal to the average value of the frictional shear stress τ' during controlled fibre pull-out. The scatter of points about a straight line indicates that the presence of PMMA at the interface has increased the value of τ' from about 5 MN m^{-2} to 10 MN m^{-2}.

These values for the frictional shear stress are about one-half of the values of the limiting interfacial shear stress, τ_0, for the two fibrous composites.

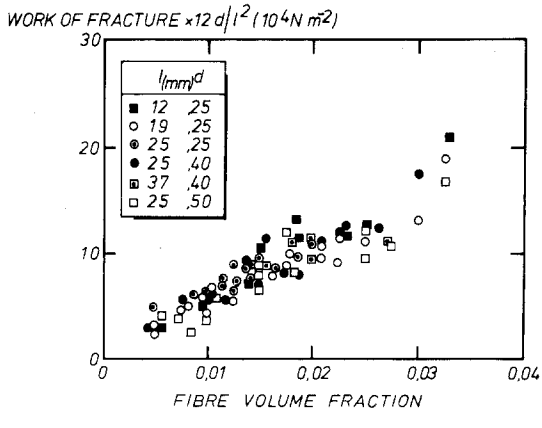

Figure 15 All the work of fracture data for concrete normalized with respect to diameter and length of fibre and plotted against fibre volume fraction. A least squares fit to the data produces a slope equivalent to $\tau' = 5$ MNm^{-2}.

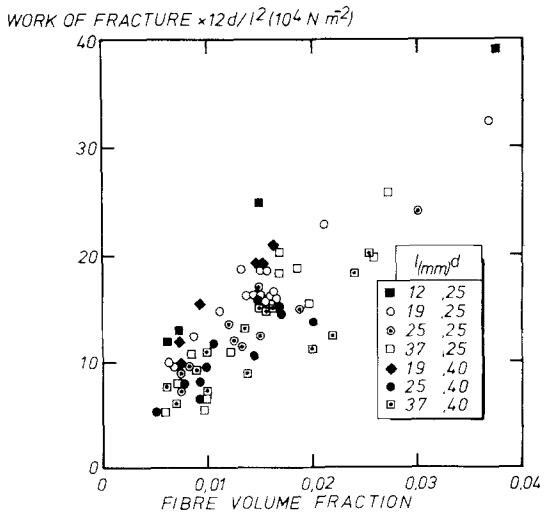

Figure 16 All the work of fracture data for PMMA concrete normalized with respect to diameter and length of fibre and plotted against fibre volume fraction. A least squares fit to the data produces a slope equivalent to $\tau' = 10\,\mathrm{MN\,m^{-2}}$.

5. Summary and conclusions

The stress for the onset of cracking in concrete can be increased by about a factor of three by impregnating the concrete with PMMA. This has the effect of reducing the amount of porosity, increasing Young's modulus, and raising the fracture surface energy of the brittle solid by an order of magnitude. A study of the effects of PMMA on the fibre debonding and fibre pull-out stresses provided equations of the form developed by Takaku and Arridge for steel wire in epoxy resin, and Pinchin for steel wire in cement. The models by Aveston *et al.* and Aveston and Kelly provided a reasonable description of the first cracking stress and post-cracking stress of the discontinuous fibrous composites, and showed that the increased resistance to cracking of the polymer–concrete composites was due to the effect of the PMMA on the strength of the fibre–matrix interface and fracture surface energy of the concrete. Work of fracture of the two kinds of composites can be explained in terms of the work done in overcoming friction during fibre pull-out; and the greater toughness of the reinforced polymer–concrete composite was due to the increase in interfacial frictional shear stress by a factor of 2. Exposure of the PMMA-impregnated composite to sea water followed by freezing and thawing had no effect on the post-cracking strength and fracture toughness.

Our approach has been to use existing models and to make simple assumptions of certain parameters that appear in the analyses which we have been unable to measure; and to include experimental values which we have been able to measure or estimate reasonably accurately. This approach utilizes the most that model-based theory has to offer but still attempting a reasonable description of the experimental data.

Acknowledgements

We would like to thank the U.S. Department of Commerce for the financial support on their Sea Grant Program SGP-2-108 and 2-35208. We are also indebted to the Bureau of Reclamation, Engineering and Research Center, Denver, Colorado, for supplying us with the polymer-impregnated concrete and to Batelle-Northwest Laboratories for supplying the fibre-reinforced concrete. Part of this work was carried out in the Department of Materials, School of Engineering and Applied Sciences at the University of California at Los Angeles.

References

1. J. AVESTON, G. A. COOPER and A. KELLY, "The Properties of Fibre Composites" (IPC Science and Technology Press, 1971) pp. 15–24.
2. A. H. COTTRELL, *Proc. Roy. Soc.* **A282** (1964) 2.
3. A. KELLY, *ibid.* **A282** (1964) 63.
4. *Idem, ibid.* **A319** (1970) 95.
5. P. HING and G. W. GROVES, *J. Mater. Sci.* 7 (1972) 427.
6. J. L. HELFET and B. HARRIS, *ibid.* 7 (1972) 494.
7. J. O. OUTWATER and M. C. MURPHY, 26th Annual Conference on Reinforced Plastics and Composites, Division of Society of Plastics Industries (1969).
8. F. F. LANGE, *Phil. Mag.* **22** (1970) 983.
9. A. G. EVANS, *ibid.* **27** (1972) 1327.
10. J. AVESTON and A. KELLY, *J. Mater. Sci.* 8 (1973) 352.
11. A. TAKAKU and R. G. C. ARRIDGE, *J. Phys. D: Appl. Phys.* 6 (1973) 2038.
12. A. KELLY and C. ZWEBEN, *J. Mater. Sci.* **11** (1976) 582.
13. D. J. PINCHIN, Ph.D. Thesis, University of Cambridge (1977).
14. N. HADJIS and M. R. PIGGOTT, *J. Mater. Sci.* **12** (1977) 358.
15. J. AVESTON, R. A. MERCER and J. M. SILLWOOD, National Physical Laboratory Report SI No. 90/11/98 (1975).
16. J. AVESTON, R. A. MERCER and J. M. SILLWOOD, "Composites – Standards, Testing and Design" (IPC Science and Technology Press, 1974) pp. 93–103.
17. J. MORTON and G. W. GROVES, *J. Mater Sci.* **11** (1976) 617.

18. W. W. GERBERICH, Ph.D. Thesis, Lawrence Radiation Laboratory, University of California, Berkeley (1971).
19. L. B. GRESZCZUK, American Society for Testing and Materials Special Technical Publication 452 (1969) p. 49.
20. J. C. ALESZKA and P. W. R. BEAUMONT, UCLA Report No. UCLA-ENG-7396 (1973) Department of Engineering and Applied Sciences.

Received 10 October 1977 and accepted 17 January1978.